Earth and Planetary Science Letters 315-316 (2012) 30–40

Contents lists available at SciVerse ScienceDirect

Earth and Planetary Science Letters

journal homepage: www.elsevier.com/locate/epsl

A data-calibrated distribution of deglacial chronologies for the North American ice complex from glaciological modeling

Lev Tarasov [a,*], Arthur S. Dyke [b], Radford M. Neal [c], W.R. Peltier [d]

[a] Department of Physics and Physical Oceanography, Memorial University of Newfoundland and Labrador, St. John's, Canada A1B 3X7
[b] Geological Survey of Canada, Ottawa, Canada K1A 0E8
[c] Department of Statistics and Department of Computer Science, University of Toronto, Toronto, Canada M5S 3G3
[d] Department of Physics, University of Toronto, Toronto, Canada M5S 1A7

ARTICLE INFO

Article history:
Accepted 6 September 2011
Available online 5 October 2011

Editor: P. DeMenocal

Keywords:
Laurentide deglaciation
uncertainty
meltwater pulse
model calibration
glacial model
ice sheet reconstruction

ABSTRACT

Past deglacial ice sheet reconstructions have generally relied upon discipline-specific constraints with no attention given to the determination of objective confidence intervals. Reconstructions based on geophysical inversion of relative sea level (RSL) data have the advantage of large sets of proxy data but lack ice-mechanical constraints. Conversely, reconstructions based on dynamical ice sheet models are glaciologically self-consistent, but depend on poorly constrained climate forcings and sub-glacial processes.

As an example of a much better constrained methodology that computes explicit error bars, we present a distribution of high-resolution glaciologically-self-consistent deglacial histories for the North American ice complex calibrated against a large set of RSL, marine limit, and geodetic data. The history is derived from ensemble-based analyses using the 3D MUN glacial systems model and a high-resolution ice-margin chronology derived from geological and geomorphological observations. Isostatic response is computed with the VM5a viscosity structure. Bayesian calibration of the model is carried out using Markov Chain Monte Carlo methods in combination with artificial neural networks trained to the model results. The calibration provides a posterior distribution for model parameters (and thereby modeled glacial histories) given the observational data sets that takes data uncertainty into account. Final ensemble results also account for fits between computed and observed strandlines and marine limits.

Given the model (including choice of calibration parameters), input and constraint data sets, and VM5a earth rheology, we find the North American contribution to mwp1a was likely between 9.4 and 13.2 m eustatic over a 500 year interval. This is more than half of the total 16 to 26 m meltwater pulse over 500 to 700 years (with lower values being more probable) indicated by the Barbados coral record (Fairbanks, 1989; Peltier and Fairbanks, 2006) if one assumes a 5 meter living range for the Acropora Palmata coral. 20 ka ice volume for North America was likely 70.1 ± 2.0 m eustatic, or about 60% of the total contribution to eustatic sea level change. We suspect that the potentially most critical unquantified uncertainties in our analyses are those related to model structure (especially climate forcing), deglacial ice margin chronology, and earth rheology.

1. Introduction

Purely geophysical deglacial ice load reconstructions such as ICE5-G (Peltier, 2004) can, through hand tuning, obtain close fits to large suites of RSL and present-day geodetic observations. However, they lack any inherent glaciological self-consistency. Specifically, they lack any constraints concerning consistency with plausible climate chronologies, energy conservation within the ice, and the physics of ice deformation and streaming. On the other hand, most glaciological model-based reconstructions to date have relied on hand-tuning a few model parameters to a small set of constraints (*e.g.*, Charbit et al., 2007; Marshall et al., 2000; Siegert et al., 2001). Aside from the sequence of work started with Tarasov and Peltier (2002, 2004), glaciological modeling has ignored the large set of constraints available to geophysical models.

We believe that the most critical deficiency is that no established reconstruction has any associated error bars. They do not take into account the uncertainties in the constraints they use nor in the models employed in any formal way. Given the large changes between the ICE4-G (Peltier, 1994) and ICE5-G (Peltier, 2004) reconstructions and

Abbreviations: RSL, relative sea level; ML, marine limit; Rdot, present-day rate of vertical uplift; LGM, last glacial maximum; mwp1a, meltwater pulse 1a; mESL, m eustatic sea level equivalent; GSM, glacial systems model; MCMC, Markov Chain Monte Carlo.

* Corresponding author. Tel.: +1 709 864 2675; fax: +1 709 864 8739.
E-mail address: lev@mun.ca (L. Tarasov).
URL: http://www.physics.mun.ca/lev/ (L. Tarasov).

0012-821X/$ – see front matter © 2011 Elsevier B.V. All rights reserved.
doi:10.1016/j.epsl.2011.09.010

the differences between those reconstructions and the geophysical ANU reconstruction,[1] it can be inferred that error bars on these reconstructions are potentially large.

As a more integrative approach, we treat determination of past ice sheet evolution as a Bayesian statistical inference problem. Specifically, we compute a probability distribution for past evolution given the physics represented in computational models along with the constraints imposed by field observations. The intent is to combine modeling and a large set of observations in a statistically rigorous manner to generate posterior probability distributions for past ice sheet evolution given the model and data.

Two related issues of current concern can also be addressed by applying this methodology to the last deglaciation of the North American ice complex. The magnitude of the contribution from each ice sheet to the meltwater pulse 1a (mwp1a) event has generated much controversy with conflicting claims continuing in the literature (Ackert et al., 2007; Bentley et al., 2010; Carlson, 2009; Clark et al., 2002; Licht, 2004; Peltier, 2005). This is not only critical for disentangling the impact of such a large fresh water flux on the climate system, but also provides some bounds on the dynamical stability of the West Antarctic Ice Sheet. This stability can also be partly constrained by better constraints on the Last Glacial Maximum (LGM) global distribution of ice.

In this paper, we briefly present the methodology and constraint data set, along with a summary of the probability distribution for the deglaciation of the North American ice complex. We focus some attention on confidence intervals for the North American contributions to 20 ka ice volume (*i.e.* the tail end of the LGM interval) and the meltwater pulse 1a (mwp1a) event.

2. Methods

The methodology is comprised of four components: the physics based model, the set of observational constraints, the metric or measuring stick for quantifying model misfit to data, and the calibration methodology for combining the first three components.

2.1. Model description

The glacial systems model (GSM) includes a 3D thermo-mechanically coupled ice sheet model, visco-elastic bedrock response, fully coupled surface drainage solver, parameterized climate forcing, surface mass-balance and calving modules, and gravitationally-self-consistent relative sea level (RSL) solver. The ice sheet model uses the shallow-ice approximation, with a Weertman type power law (*i.e.* basal velocity proportional to a power of driving stress) for basal sliding (exponent 3) and till-deformation (exponent 1). Ice-shelves are also represented by a Weertman type relation but with a square root dependence on the driving stress to better approximate plug flow and maintain numerical stability near the grounding line. The thermodynamic solver for the ice is based on conservation of energy, only ignoring horizontal conduction due to the scales involved. The bed thermal model computes vertical heat conduction to a depth of 3 km and takes into account temperature offsets at exposed ground layers due to seasonal snow cover and varying thermal conductivity of thawed and frozen ground as described in Tarasov and Peltier (2007). GSM grid resolution for North America is 1.0° longitude by 0.5° latitude.

The visco-elastic solver is asynchronously coupled with the rest of the GSM (bed response computed every 100 years), and also takes into account load changes due to changes in lake levels as well as an eustatic approximation for marine load changes. RSL is computed off-line (*i.e.* after model runs are complete) and is gravitationally self-consistent except for an eustatic correction for marine load changes during transitions between marine and grounded ice conditions (as detailed in Tarasov and Peltier, 2004). Taking into account the magnitude of non-eustatic contributions to geoidal variations, the change in sign of this component between 12 and 10 ka (which will thereby partly cancel errors from the eustatic load correction), and the resultant potential impact on bed response, this approximation should result in RSL errors below (and generally well-below) 10 m after 10 ka (and diminishing to 0 at present). It is therefore relatively minimal given the magnitude of RSL paleo-observations where marine/non-marine transition effects are significant (*e.g.*, marine inundation of Hudson Bay). Rotational components of RSL are not taken into account. We have found that rotational effects are relatively insignificant for near-field RSL determination but can alter computed RSL for far-field sites by up to about 5 m. The current calibration results use the VM5a earth rheology (Peltier and Drummond, 2008), while previous calibrations were carried out with the VM2L90 (version with 90 km lithospheric thickness) earth rheology (Peltier, 1996).

The GSM is described in detail in Tarasov and Peltier (2002, 2004, 2006, 2007). Subsequent improvements and additions include the following. First, the ice calving process can now be terminated due to assumed backing up of icebergs when all drainage routes are closed. Second, a lacustrine calving module has been added that includes a thermodynamic constraint. Specifically, calving is limited to a fraction of available heat for melting within adjacent pro-glacial lake grid-cells. This fraction is a calibration parameter. Third, a lacustrine refreezing module has been added that takes into account heat transfer through surface lake ice in combination with a freezing degree-day scheme. Fourth, a marine limit diagnostic has been added to the relative sea level solver. Fifth, as detailed in the primary supplement, the timing of Heinrich events one and two are dynamically facilitated. Unlike Stokes and Tarasov (2010), no ad-hoc forcing is imposed to potentially enhance mwp1a. More details about the GSM configuration are provided in the supplement.

For the calibration, each GSM run begins in an Eemian ice-free state for North America (122 ka) under isostatic equilibrium and terminates at present day. Unlike any other glaciological or geophysical reconstruction to date that we know of, the model does not assume Eemian ground surface topography is identical to that of present-day. Instead, every complete calibration starts with an update to the Eemian topography based on the present-day topographic discrepancy between the past 3 best runs and the input topography.

2.2. Calibration data

The calibration data set comprises a large set of RSL, marine limit (ML), and present-day rate of surface uplift data (Rdot) along with an independently inferred deglacial ice margin chronology, and various strandline observations (paleo lake level indicators). Only a subset of the constraint data is used in the Markov Chain Monte Carlo (MCMC) sampling (described below) but all data is used in the final ensemble scoring.

RSL data for North America (Dyke, unpublished data) is aggregated into 512 sites in the database. To offset calibration bias due to highly variable data density, each site is then weighted as a function of the square root of the regional and local data-point densities. Specifically, the relative site weight is the square root (number of data-points at site)/square root (sum of regional number of data-points). For example, 10 sites of 100 data-points within a region will have a total weight of $\sqrt{10}$ times the weight of a single site of 1000 data-points in one region. Weights for the subset of RSL data used in the MCMC sampling are shown in Fig. 1. The weights were computed using 10 degree longitude by 5 degree latitude grid boxes (approximate scale size of visco-elastic response) final weights were value was the average of 4 such grid box computations subject to 5 degree longitude and 2.5

[1] Lambeck, unpublished, comparison with ICE6-G shown at: https://pmip3.lsce.ipsl.fr/wiki/lib/exe/fetch.php/pmip3:design:21k:icesheet:gnh5.pdf.

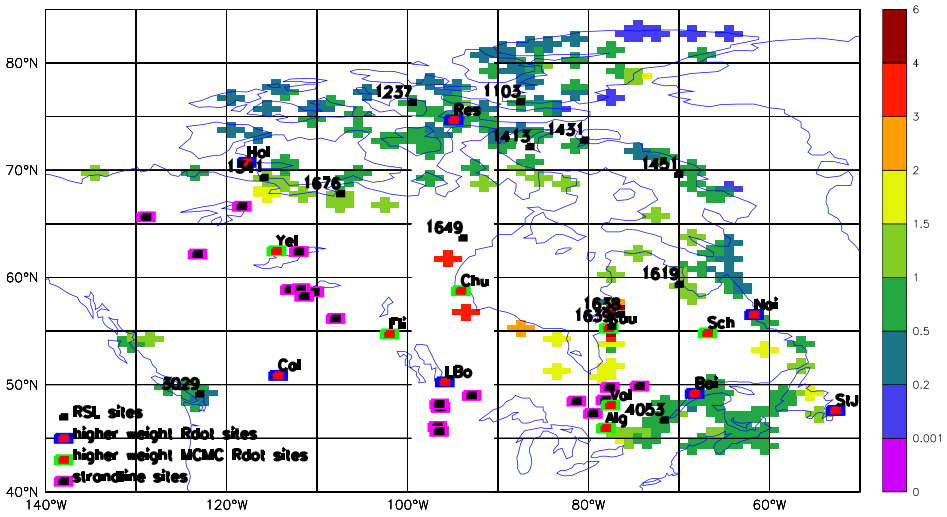

Fig. 1. Selection of calibration data locations. Not included are the marine limit (ML) data and margin chronology. To avoid clutter, only the spatially separated higher quality subset of RSL and present day geodetic data are shown. Color key indicates relative weighting of RSL sites (shaded crosses) for MCMC sampling. The 2 Southeast Hudson Bay sites (1638, 1639) were given a further factor of three weighting due to their quality.

degree latitude shifts of the grid to limit grid dependence of the weight determination. As is clear in Fig. 1, RSL data density is far from uniform.

The ML data-set (Dyke et al., 2005) covers 920 sites and is also subject to the inverse areal density weighting scheme. None of the ML data is used in the MCMC sampling. We were unable to adequately emulate model predictions for ML, likely due to the high sensitivity of ML to ice margin location. Model fits to marine limit data are therefore only part of the final ensemble scoring.

The set of data for present-day rates of uplift have also evolved over time. Currently we use near-field data from Argus and Peltier (2010). Values for 7 sites (shown in Fig. 1, chosen on the basis of largest magnitudes, tight error bars, and spatial separation from RSL data) are used in the MCMC sampling. These sites along with 7 other sites (also shown in Fig. 1) which have the next best fits to the above selection criteria, were given higher metric weights (of factor 2 except factor 6 for site Yel, factor 4 for Sch, and factor 3 for Alg and Val). The whole set of 110 sites is used in the final ensemble scoring.

The 17 strandline constraint sites are shown in Fig. 1. Values for most of the sites are listed in Tarasov and Peltier (2006), with the addition of 5 new sites for glacial lakes Barlow and Ojibway from Veillette (1994). Given the lack of dates in the data source, maximum strandline elevations from the GSM runs for these new sites over the whole deglacial interval are used. Uncertainty ranges were set to the maximum range of nearby strandline values. Similar to the case of ML data, we were unable to adequately emulate model predictions for strandline elevation. Therefore strandline data is only used in the final ensemble scoring.

2.3. Ice margin chronology and forcing

The ice margin chronology is derived from (Dyke, 2004; Dyke et al., 2003) using the INTCAL04 ^{14}C to calendar year conversion of Reimer et al. (2004). Given the partially lobate structure of the geologically inferred ice margin, as well as the high sensitivity of ice margin location to what will invariably be a poorly constrained climate forcing, it is unlikely that any glacial systems model will ever freely approach inferred margin chronologies to the degree required for accurate modeling of proglacial lakes (required for strandline predictions) and surface drainage. As such, a margin forcing is imposed whereby corrections to surface mass-balance components within what we judge to be uncertainties in the climate forcing are imposed dynamically when computed ice margin locations are beyond specified bounds. Originally a ± 80 to 100 km uncertainty interval was imposed on each isochrone. As the largest source of uncertainty is in the margin dating, a more appropriate uncertainty interval should be based on temporal uncertainty. This has now been implemented as a ± 250 to 1000 year uncertainty. Two chronologies are used, the weightings of which are under calibration control. For the chronology with wider uncertainty, time-slices for radiocarbon ages 9 ka and before (unless otherwise specified, ages are calendar years before present) have error bars corresponding to ± 1 kyr ^{14}C time-slices; subsequent time-slices mostly have ± 500 year ^{14}C uncertainty except where a single time-slice uncertainty is imposed at 8.27 ka when the final drainage of glacial Lake Agassiz is considered well dated both locally and globally. The second narrower uncertainty chronology is as above but with a maximum ± 500 year ^{14}C uncertainty.

For use in the calibration, the margin chronology is transformed to a rasterized digital map with 5 values, an example of which is shown in Fig. 2. These values are determined as follows. Raster zone 0 is for grid cells with no ice in any of the associated time-slices within the temporal uncertainty. Raster zone 1 is for grid cells with ice in at least one of the associated time slices and that are within 80 km (*i.e.* 1 grid cell) of zone 0. Raster zones 3 and 4 are assigned to grid-cells which have ice in all the associated time-slices, and are respectively within and beyond 225 km of zone 0. The remaining grid-cells are defined as zone 2. Ablation is strongly enforced in region 0, while region 1 has a weaker amount of enforced ablation, controlled by an ensemble parameter. Regions 3 and 4 have had a range of forcings, though currently the best calibration results are obtained with simple enforcement of non-negative net surface mass-balance for region 3 and no ablation for region 4. Region 2 has no margin forcing. During a model run, margin zone values are interpolated between time-slices of the rasterized margin chronology.

Given uncertainties regarding the locations of offshore ice margins (Briner et al., 2009; England et al., 2009), the zone 2 uncertainty range for marine margins was extended to the continental shelf break early in the deglaciation sequence for most regions as per discussions from the Meltwater routing and Ocean Cryosphere Atmosphere response (MOCA) network workshop at the CANQUA biennial meeting, 2009. In detail, from onset of margin forcing to 16.8 ka, it was extended for Mackenzie Delta to Banks Island and Grand Banks to the Northeast tip of Newfoundland, to 15.4 ka for the Labrador Sea and Baffin Bay, and to 13.9 ka for the rest of the Arctic.

After each surface mass-balance calculation in the model, grid-cells are checked to ensure consistency with the above conditions.

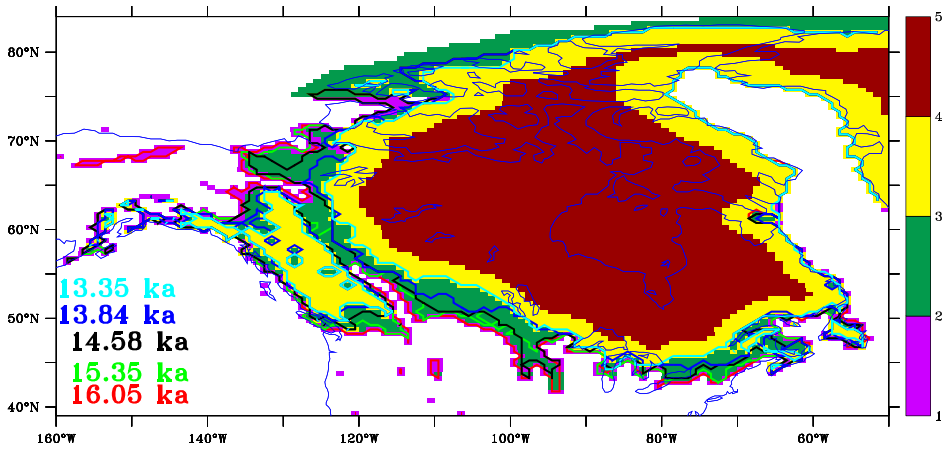

Fig. 2. 14.58 ka margin zone raster map with contours of 4 adjacent ice margins from (Dyke, 2004). This is for the version of the ice margin chronology with ±1000 year uncertainty.

Otherwise a correction is applied, one that we judge to be within the uncertainty in local climate forcing. The total number of grid-cells receiving a correction is summed over space and time, and the final value becomes part of the cost-function score value for each ensemble run. This count is disaggregated into the number of grid-cells receiving a negative mass-balance correction and those receiving a positive correction. This count is further disaggregated into three adjacent time intervals: at the onset of margin forcing, LGM in the margin chronology (*i.e.* the first time slice of 21.35 ka), and over all time-steps after 21.35 ka. As such, there are 6 separate margin forcing metric components. Inclusion of these components in the metric implies that the calibration endeavors to minimize the amount of margin forcing required and therefore select a climate forcing that is as consistent as possible with the ice margin chronology.

2.4. Calibration metric

The constraint set for the calibration is comprised of four types of observational data subject to Gaussian error models (RSL, marine limit, Rdot, and strandlines) along with a number of other components listed in Table 1. Specifically, these are the timing of the final collapse of Hudson Strait and Hudson Bay ice (between 8.6 and 8.2 ka), significant meltwater outflow into the Mississippi system (during the 14.4 to 13.7 ka time interval as indicated in the Orca Basin records) and transgression of glacial Lake Agassiz to its southern outlet at times inferred by the paleo lake level records. As well, bracketing values for ice volume at 49, 30, 26, and 20 ka along with mwp1a contributions are imposed in the metrics. Finally, as described above, the margin chronology is both an input data set and a constraint in that the integrated amount of margin forcing enters into the misfit metric.

The RSL misfit metric assumes a modified Gaussian probability distribution with standard deviation given by the values in the RSL database. Computed errors are further multiplied by a factor of 10 if they are two or more meters beyond the wrong side of a one-way error bar (*e.g.*, if computed RSL is more than 2 m below a non-intertidal mollusc or 2 m above a stump in living position). Errors are also multiplied by a factor of two for computed values outside of the given error ranges in the data-base. Finally, one-way error bars are given a default value of 50 m. The metric also computes the lowest misfit score within the temporal uncertainty of the data. This scheme has evolved over time to handle the noise in the RSL data while providing a reasonable match between subjective judgement of RSL misfits and the metric score.

Unlike RSL data, ML elevations are usually much more clearly indicated in the observational records and therefore a straightforward Gaussian error model is assumed. Pure Gaussian error models are also applied to the Rdot and strandline data-sets.

A key and poorly constrained question is the choice of the calibration metric. There is no simple objective criteria for deciding what constitutes a good ice sheet chronology when models are not able to fit all the data. The inverse areal density weightings, described in a previous subsection, address spatial density variations. The temporal correlations of data are partially addressed by aggregation into sites. By also taking into account the characteristic time-scales of bedrock response to surface load changes, one can generate order of magnitude weighting factors for the relative weights of Rdot *versus* RSL data. Especially problematic are global *versus* local data, for instance the relative weight assigned to the amount of margin forcing *versus* that assigned to RSL data fits. The non-linearity of the system also precludes the conceptually simple (though computationally challenging) solution of using the complete correlation matrix for model-data fits over some subset of past model ensembles.

Another major challenge is that the only direct ice volume constraints for paleo ice sheets are global, and contributions from the other ice sheets are also uncertain. The calibration of all ice sheets is ongoing, and given the complexity of each ice sheet, each is being calibrated individually. Global constraints along with periodically revised confidence intervals for the contributions from other ice sheets are taken into account in setting the ice volume constraints

Table 1
Secondary constraints summary, not including the main data-set constraints displayed in Fig. 1, nor the margin forcing metric components described in the previous subsection. The MCMC sampling was carried out with both weaker and tighter constraint ranges (as compared to those listed here) to ensure better coverage of the relevant parameter space. Volume ranges were derived from consideration of far-field RSL records (Fairbanks, 1989; Peltier and Fairbanks, 2006) and from the analyses of Waelbroeck et al. (2002), past hand-tuned glaciological modeling of Greenland ice sheet evolution (Tarasov and Peltier, 2002) along with past results for ongoing calibrations of the Eurasian and Antarctic deglaciation. Linear misfit metrics were imposed within the penalty intervals of the acceptance range. Of the constraints below, only the Hudson Bay deglaciation and Gulf of Mexico discharge acceptance thresholds are applied to the median, cut3, and cut3M data sieves (described in the Results and discussion section).

Constraint	Acceptance range	Non-penalty range
20 ka ice volume	>69 mESL	>76.5 mESL
26 ka ice volume	>73 mESL	>86 mESL
30 ka ice volume	39–80 mESL	43 to 75 mESL
49 ka ice volume	>19 mESL	>45 mESL
mwp1a contribution	>7 mESL	>9.5 mESL
Time of central Hudson Bay deglaciation	≥8.6 ka	>8.4 ka
Time of mid-Hudson Strait deglaciation	>10.1 ka	>9.8 ka
Meltwater discharge to Gulf of Mexico	>0.5 dSv	>1.5 dSv

for the North American calibration. Current values for the ice volume constraints are given in Table 1.

One way to partially address the above issues is to calibrate against a range of metrics. The MCMC sampling is generally carried out using metrics with different acceptance thresholds. Specifically, the thresholds are varied between weak and strong bounds as compared to the median bounds listed in Table 1. When generating final ensemble mean and variance fields, sensitivities to metric choices are then examined. Increased confidence arises from results that are relatively insensitive to the detailed weighting within the metric.

When computing final results under the full metric (as opposed to data sieving analyses further below), ensembles are first sieved with respect to minimal acceptance range constraints given in Table 1. Model runs that do not pass these constraints are rejected. The surviving ensemble score components are then normalized to unit variance across the whole ensemble (*i.e.* each of total RSL score, ML score, volume, strandline fits, Rdot score, *etc.*, are renormalized across the surviving ensemble). Normalized scores are then re-weighted to chosen ratios (the standard metric uses a 20:10:4:3:4:3 relative weighting for RSL:ML:Rdot:strandlines:margin forcing:remainder). Finally, ensemble results (weighted means and variances) are generated assuming a Gaussian distribution with noise parameter chosen to ensure that at least 100 runs are required to capture 90% of the total weight.

2.5. Calibration procedure

The GSM is presently assigned 39 calibration/ensemble parameters as listed in Tables 1 and 2 in the primary supplement. These are varied within the calibration to account for uncertainties in the model. The majority of these parameters are related to the parameterized climate forcing, the least constrained component of the GSM. Each ensemble run is defined by a parameter vector comprised of the 39 calibration parameter values for the GSM.

The calibration has evolved as an embedded series of iterations. Given a set of constraint data, ensemble parameters, and a model configuration, a random ensemble of order 3000 model runs is first generated. The parameter vectors for this random ensemble are generated as a Latin Hypercube with a prior distribution derived from previous work (be it calibration or sensitivity studies of model response to parameter variation). These model runs are then used to train artificial Bayesian neural networks (Neal, 1996), which then emulate the calibration data relevant response of the GSM to variations in calibration parameters. For example, there are a set of neural networks that predict the RSL chronologies resulting from a GSM run for a given set of calibration parameters. The neural networks can be thought of as non-linear regressors for the model response given input calibration parameters. Each neural network thereby predicts model response for MCMC sampling of model fit to a subset of the constraints. We use the slice sampling (Neal, 2003) algorithm for MCMC sampling. A subset of the converged distribution of parameters from this sampling are then used to generate a new ensemble with the full GSM. The cumulative set of model results is then used to retrain the ANN emulators. This sequence is repeated until convergence (or modeler exhaustion), usually taking about three to six iterations.

After convergence of the MCMC iterations, the full set of GSM results is scored with the metric against the complete set of calibration constraints, to generate ensemble expectations and standard deviations. A full description and validation of the calibration procedure will soon be submitted for publication.

This calibration procedure is further embedded in another iteration. Persistent misfits and the availability of new and/or revised constraints periodically necessitate a reconfiguration of the model and repeat of the whole calibration sequence. This has been the most challenging and time consuming component of this calibration, which has evolved from an initial set of 20 parameters to the presently used 39 parameters for North America as listed in Tables 1 and 2 in the primary supplement. 24 of these parameters control the climate forcing, and another 6 control the margin forcing, 4 control calving, and 5 are related to ice dynamics (fast flow due to subglacial till deformation, basal sliding, …).

3. Results and discussion

We focus on the “N5a” ensemble which is the final iteration of the current calibration and contains ten thousand model runs. Only individual runs are glaciologically self-consistent. Ensemble results are, as such, best interpreted as probabilistic descriptions. Fits for 3 example model runs to strandline constraints and the 8 highest weighted Rdot constraints are provided in the primary supplement.

3.1. RSL fits

Ensemble RSL chronologies capture the observational record within the two sigma error bars indicated for most but not all sites (Figs. 3, 4, and the RSL supplement). Unlike non-RSL error bars in this paper, RSL error bars are generated by running the two sigma upper and lower magnitude ensemble bounds of the 4D ice chronologies through the sea level solver. As such, they do not represent an individual run, only the predicted RSL chronology for an ice chronology that is everywhere and at all times either the two sigma lower or upper bound of the ensemble. The ice volume of this lower bound diagnostic ice chronology is therefore unsurprisingly below the two sigma lower bound for the ice volume chronologies of the ensemble members (Fig. 7).

Given the ambiguities discussed above in defining a calibration metric, the concept of a best run is problematic. However, as ensemble means are not glaciologically self-consistent, individual runs need examination. The single run (nn9927, with detailed plots and tabulated summary characteristics in the tertiary supplement) had the best score with any of our standard metrics even when further subject to the requirement of having the 4 main metric component values each in the top tertile for the ensemble, denoted as the “cut3” sieve. The only other conditions this sieve imposes are the acceptance thresholds for Hudson Bay deglaciation and Gulf of Mexico discharge given in Table 1. Except for the Sch site, its Rdot values are within the two sigma range (and mostly within the one sigma range) of observed values for the 14 higher weighted sites. The more complete set of RSL plots in the RSL supplement shows that the ensemble mean RSL is generally close to that of nn9927.

The difficulties in satisfying the large and diverse set of constraints with even 39 calibration parameters are evident when examining RSL fits to individual sites. Run nn9927 has a tendency to excessive RSL values compared to observations for many sites (Figs. 3 and 4). This tendency has been a persistent challenge in both the current and past calibrations. As can be seen in the expanded set of RSL chronologies in the RSL supplement, the ensemble mean captures the upper bound of most sites aside from those in Ellesmere and Axel Heiberg Island. The ensemble two sigma lower bound generally brackets the RSL observation envelope and for many sites provides a close fit to the envelope.

Given the subjectivity involved in choosing the metric, an important issue is the sensitivity of the probability distribution to the metric choice. In this context, it is worth noting that the unweighted average of the 500 best scoring runs produces a generally insignificant change to the RSL bounds indicated (not shown).

Ensemble parameter vectors can be found with much better fits to the RSL record, but at the cost of 26 ka ice volumes that are less than 64 m eustatic sea level equivalent (mESL) and as such impossible to fit far-field RSL records (Peltier and Fairbanks, 2006) given current constraints on the contributions from the other ice sheets. ML fits are fairly well correlated with RSL fits, and the best ML fits are also obtained with these low volume runs. Intriguingly, some of these best RSL score runs (*i.e.* with insufficient ice volume) attain very

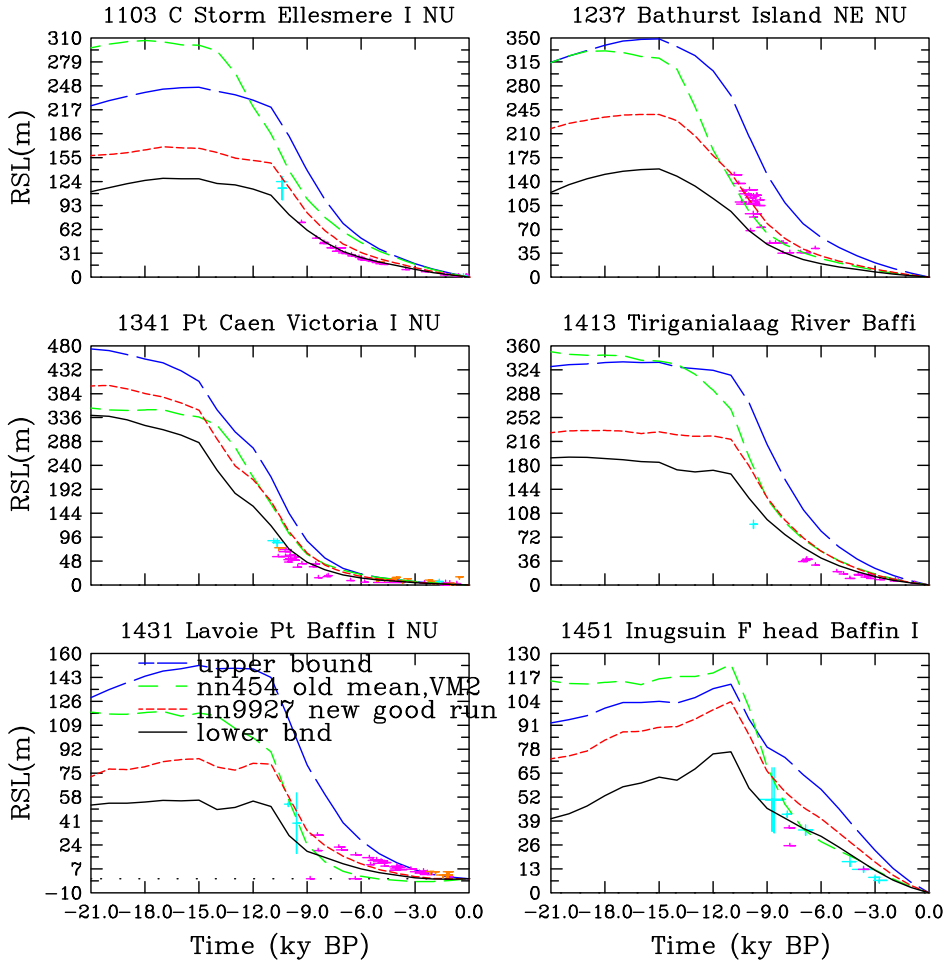

Fig. 3. Computed relative sea level chronologies for 6 high quality high arctic sites. The older nn454 weighted mean ensemble is from the previous calibration using the old spatially based definition for margin uncertainty as described in the text. Observed RSL data-points are colour coded according to their uncertainties: two-way (light blue, *e.g.*, inter-tidal molluscs such as Portlandia), one-way lower-bounding (mauve, other molluscs), one-way upper bounding (orange, *e.g.*, peat). Also note that one-way error bars are in fact generally indeterminate in their non-bounded direction, though not shown as such to avoid clutter.

good Rdot scores. However all low volume best RSL score runs have very poor strandline fits (not shown). This emphasizes the importance of imposing the full heterogeneous set of constraints in the calibration.

Especially disconcerting is the weak fit to the data-rich southeast Hudson Bay sites (1638 and 1639). Extrapolating the strong linear trend from Fig. 7 in Tarasov and Peltier (2004), regional Hudson Bay RSL error was minimized for the model configuration in that work with a regional LGM ice thickness of only 1500 m. With open water conditions through some of the main high Arctic channels along with a brute force limiting of Hudson Bay ice thickness to 1.5 km during 17–16.5 ka and down to 1 km during the 12.5–11.6 ka interval, a much closer fit to Hudson Bay and some of the high arctic RSL records was obtained (Tarasov and Peltier, 2004). This is about half of the corresponding mean ice thickness for central Hudson Bay in model run nn9927. The previous calibration also obtained a better RSL fit for Hudson Bay ("nn454 old mean, VM2" in Figs. 3 and 4), but with complete deglaciation of Hudson Strait by 12 ka and only a remnant ice shelf over most of Hudson Bay by 9 ka, contrary to geological inferences. 16 ka ice thickness for central Hudson Bay in nn454 was about 2400 m. We have been unable to create a model that can dynamically (*i.e.* without ad-hoc brute force reduction of ice) produce thin enough ice over the Hudson Bay region to fit the local RSL record, while retaining adequate grounded ice cover to hold back glacial Lakes Agassiz and Ojibway until the 8.2 ka event.

After over 50,000 model runs, we do not believe the persistent RSL misfits are due to non-optimal calibration parameters. Instead, we identify five major potential sources of uncertainty and model error. First, even with 30 climate related calibration parameters, the climate forcing must be a far cry from reality. However, given the presence of margin forcing, and the inclusion of the amount of margin forcing required in the total misfit metric, it is unclear to us how a much more physically based climate forcing could significantly improve RSL fits without worsening fits to other components of the metric.

A source of error in the model that could have more impact on RSL fits is the use of the shallow ice approximation. This approximation ignores longitudinal and horizontal shear stresses which are known to be significant or dominant for ice shelves and most ice-streams. Whether inclusion of these stress components can produce the large draw-downs apparently required to fit the Hudson Bay RSL records is currently under investigation.

A third source of uncertainty is that the visco-elastic model assumes a linear and spherically symmetric visco-elastic structure. The extent to which this simplification affects model response and computed RSL chronologies has yet to be quantified. Also problematic is the lack of error bars for presently available earth rheologies.

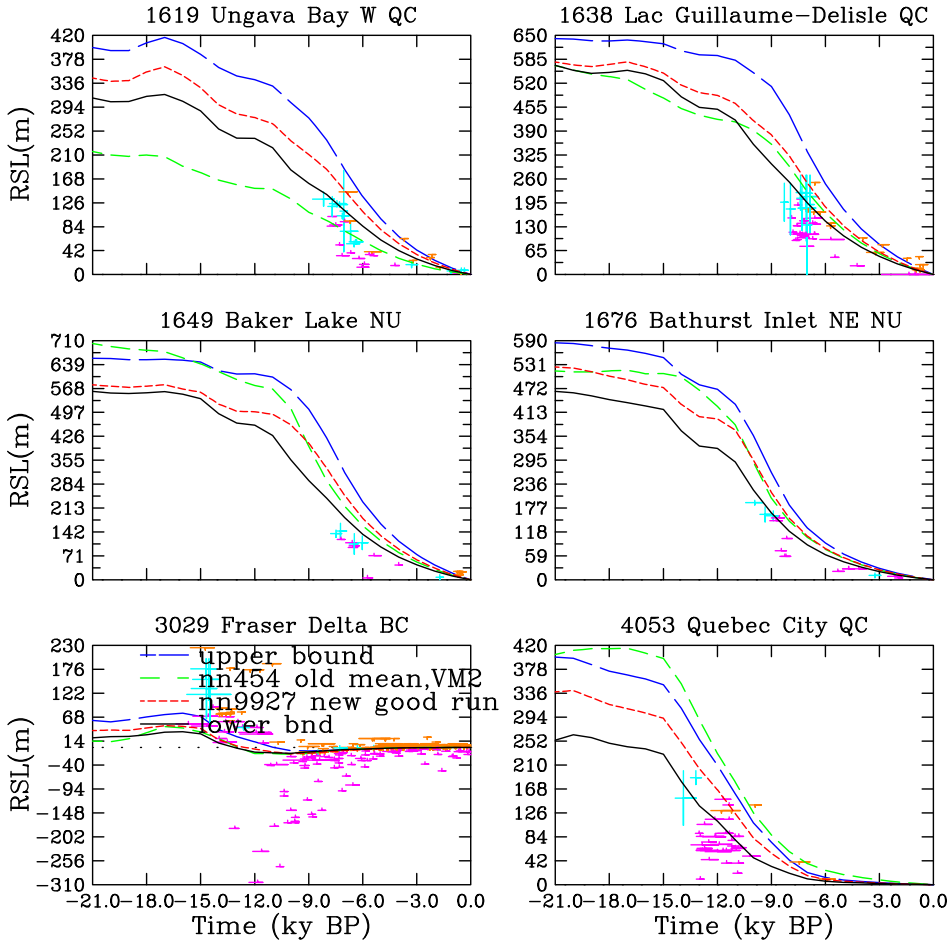

Fig. 4. Computed relative sea level chronologies for 6 high quality non-high arctic sites as per the previous figure.

The model resolution is a fourth source of error. Many of the smaller Arctic ice streams are not resolved with the given grid resolution and this likely accounts for some of the excessive RSL predictions for those regions.

Finally, the margin chronology has weak control over many regions. The chosen temporally based uncertainty specification is a more defensible choice than the previous spatially based uncertainty choice. However, what is really needed is a focused collaboration among the glacial geological community to create maximum and minimum bounds for each isochrone and to update the Dyke (2004) margin chronology.

3.2. 20 ka fields and mwp1a contributions

The ensemble mean basal velocity and topography shown in Fig. 5 are again not representative of a single glaciologically-self-consistent model run. The weighted averaging also blurs ice stream locations

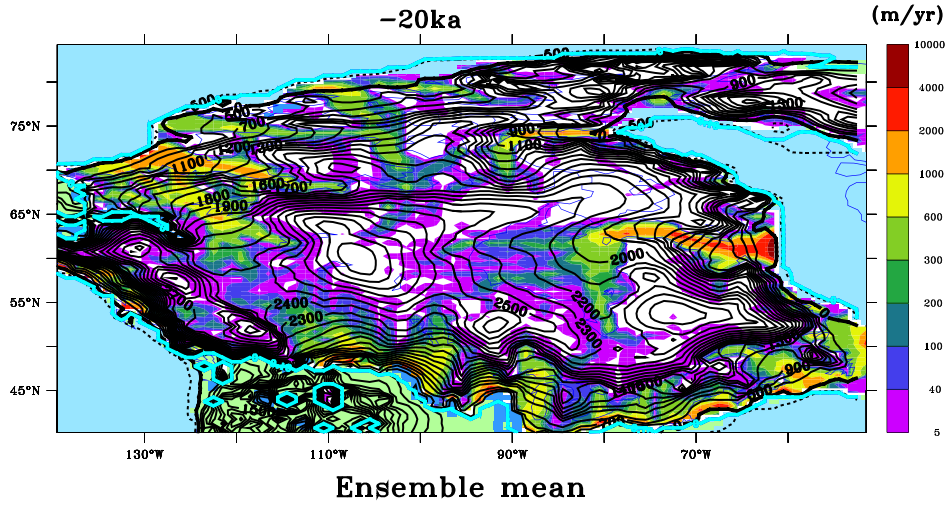

Fig. 5. Weighted mean basal velocity and surface elevation for ensemble N5a.

and magnitudes and smooths ice topography. It is simply the expectation value and must be interpreted as such. The mean does capture the major ice-streams; an initial comparison of the ice-stream structure from the previous calibration against independent geological inferences (Stokes and Tarasov, 2010) has shown a reasonable match. The topographic structure also captures most of the key features of geologically inferred reconstruction of Dyke and Prest (1987) aside from the lack of a distinct Foxe dome for this isochrone. A distinct dome does appear after 11 ka in the ensemble mean (Fig. 13 in the primary supplement) and a somewhat more penetrative ice stream along Prince Regent Inlet-Lancaster Sound would generate a Foxe Dome at LGM.

An uncertainty estimation for 20 ka ice thickness is shown with the two sigma range from the ensemble in Fig. 6. The largest variations indicated are due to inter-model variations in ice streaming. The uncertainty map reflects the extent to which the model is regionally constrained by the data set and not the complete possible range of error in ice thickness. For instance, from the discussion of RSL fit in the previous subsection, the regional Hudson Bay ice thickness from the ensemble is possibly a kilometer too thick. However, given that the model is unable to dynamically generate thin ice while meeting all hard constraints, the ensemble variance for this region is mostly less than 600 m. Therefore, the uncertainty map provides a component of the total error but not the complete error. It does provide a useful guide to determining in what regions (and for what time periods when considering the whole chronology provided in the primary supplement) new constraint data would be most useful.

The comparison of North American ice volume chronologies shown in Fig. 7 demonstrates the relative robustness of the ice volume expectation values to metric definition during the deglacial interval. The fully scored N5a ensemble ("N5a"), a variant thereof with a full third of the metric weight assigned to margin forcing (not shown), and the raw average of the cut3 sieved ensemble (as detailed in the figure caption) have nearly indistinguishable chronologies following the onset of margin forcing.

Confidence intervals for 20 ka North American ice volume can be read directly from the ensemble ice volume chronology. A value of 70.1 ± 2.0 mESL captures the ranges for the standard metrics with and without additional cut3 sieving (the latter just narrows the uncertainty ranges). This also nearly brackets the uncertainty range if no mwp1a, 20 ka, and 26 ka ice volume constraints are included in the metric applied to the cut3 sieved data set (69.5 ± 1.6 mESL). The MCMC sampling was biased towards higher values (in order to more easily fit far-field constraints), which is evident in the higher value of the unweighted (*i.e.* non-scored) ensemble average for

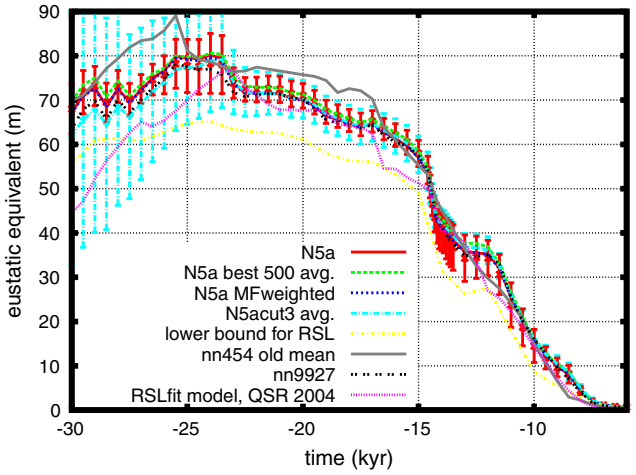

Fig. 7. Deglacial ice volume chronologies in eustatic equivalent meters of sea level (conversion factor of 25.19 m per 10^{15} m^3 of ice. The two chronologies with explicit "avg." labels are unweighted averages. N5acut3 only includes ensemble N5a runs that are in the top tertile for each of the four main metric components (RSL, ML, Rdot, strandlines), that have final collapse of the Hudson Bay ice dome after 8.6 ka, and that have at least 0.5 dSv discharge of meltwater into the Gulf of Mexico during the 14.4 ka to 13.7 ka interval. No ice volume thresholds are imposed on this sieve. The "lower bound for RSL" chronology is the ice volume of the 2 sigma lower bound ice thickness chronology used to generate the lower bound RSL in Figs. 3 and 4. Sigma confidence intervals for ensemble N5a and N5acut3 are shown).

20 ka ice volume (73.9 ± 4.0) when only subject to median sieving (*i.e.* rejection if any of the RSL, Rdot, ML, and strandline scores are below their ensemble median). This demonstrates the role of the constraint data set in limiting what many in the sea level research community would see as a low value for 20 ka ice volume. Furthermore, the tendency to excessive RSL predictions implies that if anything the ensemble results are an upper bound.

The critical role of the ice margin chronology in constraining ice volume is evident in Fig. 7. Much wider confidence intervals occur prior to the onset of the margin forcing especially for the cut3 average chronology (*i.e.* no application of metric). The ensemble is able to obtain a larger 26 ka ice volume (compared to that of 20 ka) which is required in order to fit far-field RSL records (Peltier and Fairbanks, 2006) given current constraints on contributions from other ice sheets. However, this larger 26 ka ice volume is at least partly due to ice extent penetrating beyond LGM bounds (future calibrations will enforce no ice beyond LGM limits throughout the 30 to 21 ka interval).

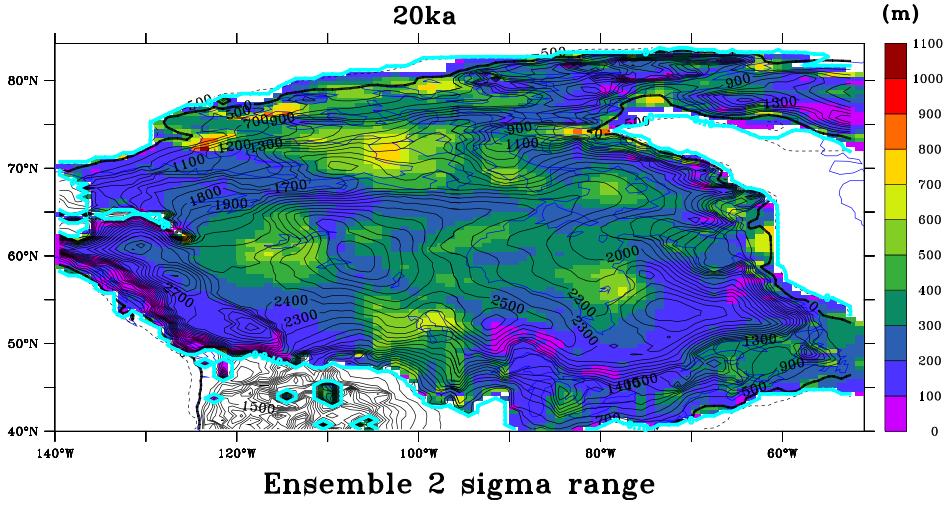

Fig. 6. One-way 2 sigma range for ensemble N5a ice thickness at 20 ka.

The ice volume chronology comparison also documents the evolution of calibration results from the initial study of Tarasov and Peltier (2004). The best RSL fitting ("RSLfit") model from that study had an ad-hoc Heinrich Event 1 forcing that reduced central Hudson Bay ice thickness to 1500 m, with an evident large reduction of ice volume at that time compared to other runs. That study also lacked any pre-21 ka ice volume constraints and only used RSL and a handful of Rdot data. The nn454 ("old mean") chronology from the previous calibration, as described above, had stronger 26 ka and 21 ka minimum ice volume thresholds imposed.

With the given margin chronology and climate forcing, the 500 year interval of maximum ice loss is 14.6 to 14.1 ka. Mean and two sigma bounds for mwp1a contributions were extracted from the ensemble over this interval. Ensemble mwp1a contributions are 11.65 ± 1.6 m eustatic with the standard metric and 11.63 ± 1.6 if the mwp1a rejection and penalty ranges in Table 1 are ignored. As such, reject/penalty ranges for mwp1a have insignificant impact on the results. Extending the lower bound to 9.4 m eustatic also captures the uncertainty range for the standard metric (with no mwp1a constraint) with the cut3 sieve. Excluding both mwp1a and all ice volume constraints, the range for the standard metric is 11.8 ± 1.2 when subject to the cut3M data sieve described in the caption for Fig. 8. The largest contribution to mwp1a is from the western Laurentide sector (Keewatin and south there-of, refer to primary supplement). This is also one of the regions with the weakest chronological control for the deglacial ice margin retreat. As such, the calibrated mwp1a contribution has, to some extent, unquantified uncertainties associated with the margin chronology.

The previous calibration had a mean mwp1a contribution of only 7.0 m eustatic. We suspect that this smaller value as compared to that of the present calibration is largely due to the older spatially motivated specification of margin uncertainty (the previous calibration also had a much smaller set of Rdot constraints which might have also played a role). The zone 3 region (margin zone where no net mass-loss is enforced) for the western Laurentide sector in the old treatment retreated less over this time interval than that of the new uncertainty specification. The best runs in the new calibrated ensemble tended to have the margin forcing chronology heavily (>90%) weighted towards the chronology with a maximum of ± 500 years temporal uncertainty. Given the dating and C14 calibration uncertainties along with uncertainties relating proxy date to actual margin position, ± 500 years represents a lower bound uncertainty for nearly all sectors of the ice margin during the whole deglaciation interval (except during the well-dated 8.2 ka event).

To elucidate the extent to which metric threshold values for ice volume and mwp1a contributions biased their final distributions, one can compare single metric component values to 20 ka ice volume and mwp1a contributions without imposing any ice volume and mwp1a thresholds. This can also help isolate the role of these metric components in constraining these contributions. However, to avoid distortion of the comparison from clearly bad model runs, these comparisons are best made with sieved subsets of the ensemble. The clearest tight bound for 20 ka ice volume contribution is from marine limit fits (Fig. 8). The given sieves do not include any ice volume nor mwp1a thresholds. To present a sense of the response of sub-ensemble ranges to various data-sieves, we present results for 3 successively stronger sieves. From examination of individual runs and their associated scores, and to enforce minimal self-consistency with the climate forcing, we have chosen the strongest sieve, "cut3M", for determining bounding error bars for ensemble values. With the cut3M sieve, a clear aggregation of the lowest marine limit misfit values occurs for a range of 20 ka ice volume contributions of 68.7 to 70.8 mESL. Considering the intersection of best fit ranges under cut3M across the four major metric components (RSL, Rdot, marine limits, and strandlines, refer to primary supplement for rest of plots), one obtains a range of 69.0 to 70.7 mESL. This is within the previously stated range using the full metrics. Given that this sieve-based analysis only partially (through the cut3M sieve) takes into simultaneous account the four major metric components, we do not use this intersection range to reduce the uncertainty estimate with the full metric.

Mwp1a contributions are most strongly bounded by strandline fits. This is likely due to the temporal and spatial proximity of this data to the regions where the margin most strongly receded during mwp1a. Again taking the best fit subset under cut3M sieving (Fig. 9), a range of either 9.4 to 13.8 mESL or 9.9 to 10.7 mESL, depending on the acceptance threshold. To be cautious, we take the wider range. Again taking the intersection of the best-fit ranges under cut3M for each of the four major metric components (refer to primary supplement for plots of other components), a range of 9.4

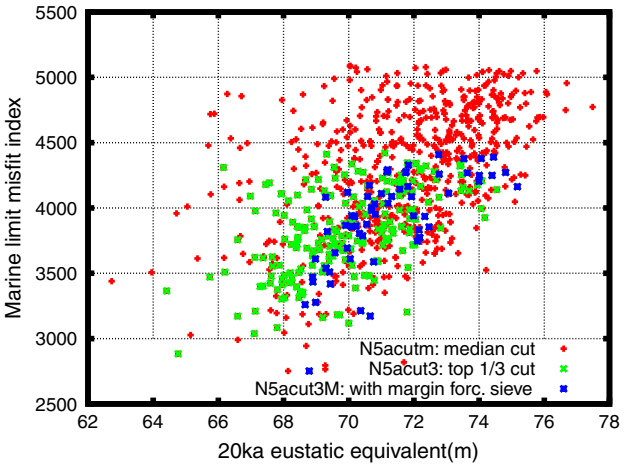

Fig. 8. Ensemble member 20 ka eustatic equivalent ice volumes *versus* marine limit misfit index (cost function value) for 3 sievings of the full ensemble. Note indicated misfit index values are a logarithmic representation of their contributions to the metric weighting (*i.e.* in analogy with the relationship between the square of a statistical residual and the corresponding probabilistic value under a Gaussian distribution). N5acutm only includes ensemble N5a runs that are better than median for each of the 4 main metric components (RSL, ML, Rdot, strandlines), that have final collapse of the Hudson Bay ice dome after 8.6 ka, and that have at least 0.5 dSv discharge of meltwater into the Gulf of Mexico during the 14.4 ka to 13.7 ka interval. The cut3 sieve is similar except that it only accepts runs in the top tertile for each main metric component. The cut3M sieve further imposes the filter of requiring lowest two thirds margin forcing (*i.e.* relative to the whole ensemble) for each of the 6 margin forcing metric components. This latter sieve is used in determining maximal ranges for 20 ka ice volume and mwp1a contributions. None of the sieving filters impose any ice volume or mwp1a contribution threshold.

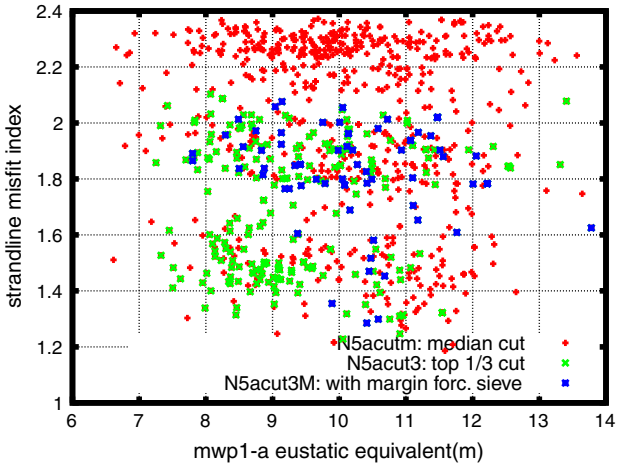

Fig. 9. Ensemble member meltwater pulse 1a contributions *versus* strandline misfit index (cost function value) for 3 sievings of the full ensemble. The sieves are as described in the caption of Fig. 8.

to 11.4 mESL is obtained. This is within the widest calibrated range (*i.e.* under various versions of the full metric) of 9.4 to 13.2 mESL for the mwp1a contribution.

4. Conclusions

We wish to emphasize that model results shown here have evolved from over 50,000 GSM runs. The associated MCMC sampling has probed hundreds of millions of parameter sets. This study incorporates a large and diverse set of constraints. The set of constraints is large enough that even the latest model configuration with 39 ensemble parameters is not able to properly cover the deglacial phase space.

Our results include confidence intervals, but they are necessarily incomplete as they lack quantification of structural model errors (*i.e.* errors due the approximations in the model, irrespective of calibration parameters). A Bayesian methodology, based on the same ANN emulator approach, has been developed for complete error specification and applied to a general circulation climate model (Hauser et al., in press). Application of that approach to the deglacial ice sheet evolution is much more technically challenging due to the indirect nature of paleo-observations. Unlike the climate modeling case, ice sheet thickness (except for sparse trim-lines and nunatuks), basal velocity magnitudes, and ice temperature fields have only an indirect relation to observable data. However, given that the majority of RSL sites are covered by the two sigma bounds from the ensemble, we believe that the results do offer reasonable though incomplete error bars for most regions.

Two other major sources of uncertainty that have yet to be quantified are that of the margin chronology and the earth rheology. As detailed above, the calibration does partially account for margin uncertainty, but certain results (such as the North American contribution to mwp1a) may well be sensitive to improvements in the chronology. The revision of the North American deglacial ice margin chronology and more accurate assessment of its errors is a key goal of the INQUA sponsored Meltwater Ocean Cryosphere Atmospheric (MOCA) network. An excellent example is that of the preliminary DATED deglacial chronology for Eurasia (R. Gyllencreutz, Jan Mangerud, John Inge Svendsen and Oystein Lohne, written communication 2010). Examination of the impacts of rheological uncertainty on North American calibration is a clear next step with consideration of inclusion of the rheological structure within the set of calibration parameters. Furthermore, the viscoelastic response model currently employed is linear and assumes a spherically symmetric earth rheology. Understanding the uncertainties arising from these latter assumptions is a longer term challenge for the community.

With these important caveats, the past 5 years of model calibration have yielded some relatively robust conclusions for the North American deglaciation. First, 20 ka ice volume is unlikely to be larger than 72 mESL nor (though with weaker confidence given the tendency for RSL over-prediction) smaller than 68 mESL. Second, North American contributions to mwp1a are likely between 9.4 and 13.2 m eustatic equivalent, with the dominant contribution coming from the western sector of the Laurentide ice sheet. Uncertainties due to model limitations are unlikely to significantly increase the 20 ka eustatic contribution given the constraint from the deglacial margin chronology and the nature of RSL misfits. Model limitations may have a stronger impact on the magnitude of the mwp1a contribution. As described earlier, changes in the specification of margin chronology uncertainty have had a significant impact on this contribution.

Consideration of the ice thickness uncertainty maps in the primary supplement permits identification of regions most in need of better constraint. We therefore hope these results will aid the field community in guiding future work as well as act as a stepping stone to expose the insights gleaned from years of close up fieldwork and perhaps challenge assumptions.

Next steps for this calibration include 3 major improvements. First, inclusion of a more advanced ice dynamics core with shallow-shelf physics and Schoof constraints at the grounding line (Pollard and DeConto, 2009). Second, a doubling of model resolution. Finally, a staged evolution of the climate component. The first step will be a much more dynamically based representation of the climate expanding on the work of Abe-Ouchi et al. (2007) with the long-term goal of a fully coupled ice and climate model calibration of the past glacial cycle.

On the data side, there is a need for a more accurate specification of ice margin chronology errors, especially in poorly constrained regions such as Keewatin. Lineations are another set of possible constraints that can be incorporated into the calibration. Our general philosophy however is to first compare and document calibrated model results against new possible constraints before considering their incorporation into the constraint data set. Finally we wish to emphasize that a limited number of quality data generating tight error bars is of much more value than a large number of noisy data with poorly defined error bars.

Acknowledgements

Support provided by Canadian Foundation for Innovation and the National Science and Engineering Research Council. This paper is a contribution to the INQUA sponsored Meltwater Ocean Cryosphere Atmospheric response network (MOCA) and has benefited from discussions within network workshops. This paper benefitted from the review comments of two anonymous reviewers. Neal and Tarasov both hold Canada Research Chairs.

Appendix A. Supplementary material

Supplementary data to this article can be found online at doi:10.1016/j.epsl.2011.09.010.

References

Abe-Ouchi, A., Segawa, T., Saito, F., 2007. Climatic conditions for modelling the Northern Hemisphere ice sheets throughout the ice age cycle. Clim. Past 3 (3), 423–438.
Ackert Jr., R.P., Mukhopadhyay, S., Parizek, B.R., Borns, H.W., 2007. Ice elevation near the West Antarctic Ice Sheet divide during the Last Glaciation. Geophys. Res. Lett. 34 (21) (NOV 10).
Argus, D.F., Peltier, W.R., 2010. Constraining models of postglacial rebound using space geodesy: a detailed assessment of model ice-5g (vm2) and its relatives. Geophys. J. Int. 181, 697–732.
Bentley, M.J., Fogwill, C.J., Le Brocq, A.M., Hubbard, A.L., Sugden, D.E., Dunai, T.J., Freeman, S.P.H.T., 2010. Deglacial history of the West Antarctic Ice Sheet in the Weddell Sea embayment: constraints on past ice volume change. Geology 38 (5), 411–414 (MAY).
Briner, J.P., Davis, P.T., Miller, G.H., 2009. Latest Pleistocene and Holocene glaciation of Baffin Island, Arctic Canada: key patterns and chronologies. Quat. Sci. Rev. 28, 2075–2087.
Carlson, A.E., 2009. Geochemical constraints on the Laurentide Ice Sheet contribution to Meltwater Pulse 1A. Quat. Sci. Rev. 28 (17–18, Sp. Iss. SI), 1625–1630 (AUG).
Charbit, S., Ritz, C., Philippon, G., Peyaud, V., Kageyama, M., 2007. Numerical reconstructions of the Northern Hemisphere ice sheets through the last glacial–interglacial cycle. Clim. Past 3 (1), 15–37.
Clark, P.U., Mitrovica, J.X., Milne, G.A., Tamisiea, M.E., 2002. Sea-level fingerprinting as a direct test for the source of global meltwater pulse 1a. Science 295, 2438–2441.
Dyke, A.S., 2004. An outline of North American deglaciation with emphasis on central and northern Canada. In: Ehlers, J., Gibbard, P.L. (Eds.), Quaternary Glaciations—Extent and Chronology, Part II, Vol. 2b. Elsevier, pp. 373–424.
Dyke, A.S., Prest, V.K., 1987. Late Wisconsinan and Holocene history of the Laurentide ice sheet. Geog. Phys. Quat. 41, 237–264.
Dyke, A.S., Moore, A., Robertson, L., 2003. Deglaciation of North America. Tech. Rep. Open File 1574, Geological Survey of Canada, Thirty-Two Maps at 1:7 000 000 Scale with Accompanying Digital Chronological Database and One Poster (in Two Sheets) with Full Map Series.
Dyke, A.S., Dredge, L.A., Hodgson, D.A., 2005. North American deglacial marine- and lake-limit surfaces. Geog. Phys. Quat. 59 (2–3), 155–185.
England, J., Furze, M.F., Doupe, J.P., 2009. Revision of the NW Laurentide Ice sheet: implications for paleoclimate, the northeast extremity of Beringia, and Arctic Ocean sedimentation. Quat. Sci. Rev. 28, 1573–1596.
Fairbanks, R.G., 1989. A 17,000-year glacio-eustatic sea level record: influence of glacial melting rates on the Younger Dryas event and deep-ocean circulation. Nature 342, 637–641.

Hauser, T., Keats, A., Tarasov, L., in press. Artificial neural network assisted Bayesian calibration of climate models. Climate Dynamics.
Licht, K., 2004. The Ross Sea's contribution to eustatic sea level during meltwater pulse 1A. Sediment. Geol. 165 (3–4), 343–353 (MAR 15).
Marshall, S.J., Tarasov, L., Clarke, G.K.C., Peltier, W.R., 2000. Glaciology of Ice Age cycles: physical processes and modelling challenges. Can. J. Earth Sci. 37, 769–793.
Neal, R.M., 1996. Bayesian learning for neural networks. Lecture Notes in Statistics, 118. Springer.
Neal, R., 2003. Slice sampling. Ann. Stat. 31 (3), 705–767.
Peltier, W.R., 1994. Ice age paleotopography. Science 265, 195–201.
Peltier, W.R., 1996. Mantle viscosity and ice age ice sheet topography. Science 273, 1359–1364.
Peltier, W.R., 2004. Global glacial isostatic adjustment and the surface of the ice-age Earth: the ICE-5G(VM2) model and GRACE. Annu. Rev. Earth Planet. Sci. 32, 111–149.
Peltier, W.R., 2005. On the hemispheric origins of meltwater pulse 1a. Quat. Sci. Rev. 24 (14–15), 1655–1671.
Peltier, W.R., Drummond, R., 2008. Rheological stratification of the lithosphere: a direct inference based upon the geodetically observed pattern of the glacial isostatic adjustment of the North American continent. Geophys. Res. Lett. 35 (L16314). doi:10.1029/2008GL034586.
Peltier, W.R., Fairbanks, F.G., 2006. Global glacial ice volume and last glacial maximum duration from an extended Barbados sea level record. Quat. Sci. Rev. 25, 3322–3337.
Pollard, D., DeConto, R.M., 2009. Modelling West Antarctic ice sheet growth and collapse through the past five million years. Nature 458, 329–332. doi:10.1038/nature07809.
Reimer, P.J., Baillie, M.G., Bard, E., Bayliss, A., Beck, J.W., Bertrand, C., Blackwell, P.G., Buck, C.E., Burr, G., Cutler, K.B., Damon, P.E., Edwards, R.L., Fairbanks, R.G., Friedrich, M., Guilderson, T.P., Hughen, K.A., Kromer, B., McCormac, F.G., Manning, S., Ramsey, C.B., Reimer, R.W., Remmele, S., Southon, J.R., Stuiver, M., Talamo, S., Taylor, F.W., van der Plicht, J., Weyhenmeyer, C.E., 2004. IntCal04 terrestrial radiocarbon age calibration, 26–0 ka BP. Radiocarbon 46, 1029–1058.
Siegert, M., Dowdeswell, J., Hald, M., Svendsen, J., 2001. Modelling the Eurasian Ice Sheet through a full (Weichselian) glacial cycle. Global Planet. Change 31 (1–4, Sp. Iss. SI), 367–385 (NOV).
Stokes, C., Tarasov, L., 2010. Ice streaming in the Laurentide Ice Sheet: a first comparison between data-calibrated numerical model output and geological evidence. Geophys. Res. Lett. 37 (L01501).
Tarasov, L., Peltier, W.R., 2002. Greenland glacial history and local geodynamic consequences. Geophys. J. Int. 150, 198–229.
Tarasov, L., Peltier, W.R., 2004. A geophysically constrained large ensemble analysis of the deglacial history of the North American ice sheet complex. Quat. Sci. Rev. 23, 359–388.
Tarasov, L., Peltier, W.R., 2006. A calibrated deglacial drainage chronology for the North American continent: evidence of an Arctic trigger for the Younger Dryas. Quat. Sci. Rev. 25 (7–8), 659–688.
Tarasov, L., Peltier, W.R., 2007. The co-evolution of continental ice cover and permafrost extent over the last glacial–interglacial cycle in North America. JGR-Earth Surf. 112 (F02S08). doi:10.1029/2006JF000661.
Veillette, J.J., 1994. Evolution and paleohydrology of glacial lakes Barlow and Ojibway. Quat. Sci. Rev. 13, 945–971.
Waelbroeck, C., Labeyrie, L., Michel, E., Duplessy, J., McManus, J., Lambeck, K., Balbon, E., Labracherie, M., 2002. Sea-level and deep water temperature changes derived from benthic foraminifera isotopic records. Quat. Sci. Rev. 21 (1–3), 295–305.